







Article

Assessment of Oxidative Stress by Detection of H₂O₂ in Rye Samples Using a CuO- and Co₃O₄-Nanostructure-Based Electrochemical Sensor

Irena Mihailova ^{1,*}, Marina Krasovska ¹, Eriks Sledevskis ¹, Vjaceslavs Gerbreders ¹, Valdis Mizers ¹
and Andrejs Ogurcovs ^{1,2}

¹ G. Liberts' Innovative Microscopy Centre, Department of Technology, Institute of Life Sciences and Technology, Daugavpils University, Parades Street 1a, LV-5401 Daugavpils, Latvia; marina.krasovska@du.lv (M.K.); eriks.sledevskis@du.lv (E.S.); vjaceslavs.gerbreders@du.lv (V.G.); valdis.mizers@du.lv (V.M.); andrejs.ogurcovs@cfi.lu.lv (A.O.)

² Institute of Solid State Physics, University of Latvia, Kengaraga Street 8, LV-1063 Riga, Latvia

* Correspondence: irena.mihailova@du.lv; Tel.: +371-28226689

Abstract: Hydrogen peroxide is essential for biological processes and normally occurs in low concentrations in living organisms. However, exposure of plants to biotic and abiotic stressors can disrupt their defense mechanisms, resulting in oxidative stress with elevated H₂O₂ levels. This oxidative stress can damage cell membranes, impair photosynthesis, and hinder crucial plant functions. The primary focus of this article is to investigate the effects of salt and herbicide stress factors on the growth of rye samples. For precise quantification of the released H₂O₂ concentration caused by these stress factors, a non-enzymatic electrochemical sensor was developed, employing nanostructured CuO and Co₃O₄ oxides. Nanostructured electrodes exhibit high sensitivity and selectivity towards H₂O₂, making them suitable for detecting H₂O₂ in real samples with complex compositions. Rye samples exposed to NaCl- and glyphosate-induced stress demonstrated notable concentrations of released H₂O₂, displaying an increase of up to 30% compared to the control sample. Moreover, optical absorption measurements revealed a substantial decrease in chlorophyll concentration (up to 35% compared to the control group) in rye samples where elevated H₂O₂ levels were detected through electrochemical methods. These findings provide further evidence of the harmful effects of elevated H₂O₂ concentrations on plant vital functions.

Keywords: salt stress; oxidative stress; rye; electrochemical sensor; hydrogen peroxide; cobalt oxide nanostructures; copper oxide nanostructures



Citation: Mihailova, I.; Krasovska, M.; Sledevskis, E.; Gerbreders, V.; Mizers, V.; Ogurcovs, A. Assessment of Oxidative Stress by Detection of H₂O₂ in Rye Samples Using a CuO- and Co₃O₄-Nanostructure-Based Electrochemical Sensor. *Chemosensors* **2023**, *11*, 532. <https://doi.org/10.3390/chemosensors11100532>

Academic Editor: Edward P. C. Lai

Received: 6 July 2023

Revised: 6 October 2023

Accepted: 8 October 2023

Published: 10 October 2023



Copyright: © 2023 by the authors. Licensee MDPI, Basel, Switzerland. This article is an open access article distributed under the terms and conditions of the Creative Commons Attribution (CC BY) license (<https://creativecommons.org/licenses/by/4.0/>).

1. Introduction

Reactive oxygen species (ROS) in plants refer to a group of highly reactive molecules that contain oxygen and are involved in a variety of physiological processes, including plant growth, development, and responses to both biotic and abiotic stresses [1,2]. Plants produce several types of ROS, including superoxide radicals, hydrogen peroxide, singlet oxygen, and others [3–6]. These ROS molecules, when present at low levels, can serve as signaling molecules that regulate various facets of plant growth and development, encompassing cell division and differentiation [1]. Furthermore, ROS can activate defense responses in plants, enabling them to combat biotic and abiotic stressors [4]. However, an excessive accumulation of ROS can be detrimental to plants, causing oxidative stress and cellular damage [3,7]. Plant stress can affect the concentration of ROS in different ways depending on the type and intensity of the stressor. Generally, many abiotic and biotic stressors can lead to an increase in ROS production in plant cells [1].

Abiotic stress factors, like high temperatures [8], drought [9], salinity [10], exposure to herbicides, and heavy metals [11], can disrupt the delicate equilibrium between ROS

production and ROS scavenging in plants [12]. This can result in an accumulation of ROS, which can lead to oxidative damage to cellular components and impaired plant growth and development. For example, drought and salt stress can lead to the accumulation of H₂O₂ and other ROS in plant cells, which can cause osmotic stress, membrane damage, reduced photosynthesis, and impaired plant growth.

Salt stress can induce the production of H₂O₂ through multiple mechanisms [5,13]. One mechanism is through the activation of nicotinamide adenine dinucleotide phosphate (NADPH) oxidases (NOXs), which produce superoxide radicals that can be converted to H₂O₂ by superoxide dismutase (SOD) [14,15]. Another mechanism is through the disruption of photosynthetic electron transport, which can lead to the production of excess electrons and the formation of H₂O₂ by the Mehler reaction [16].

Biotic stressors, such as pathogen infection and herbivory [17], can also stimulate an increase in ROS production in plants.

Hence, it is crucial for plants to maintain a balance between ROS production and scavenging to prevent excessive oxidative stress. Plants have developed various mechanisms to regulate ROS levels, including the synthesis of antioxidant enzymes like catalase, peroxidase, and superoxide dismutase [18]. These enzymes effectively scavenge excess H₂O₂ and other ROS, mitigating oxidative stress and minimizing damage to plant cells [19]. Understanding the regulation of ROS, particularly H₂O₂, in plants is an active area of research with significant implications for comprehending plant physiology, stress responses, and the development of strategies to enhance plant growth, productivity, and stress tolerance [20,21].

There are several methods available for determining the concentration of H₂O₂ in plants. Biochemical assays [22,23] involve extracting H₂O₂ from plant tissues and quantifying its concentration using a redox-sensitive dye such as titanium sulfate or leuco crystal violet [24,25]. The dye reacts with H₂O₂, producing a colored product that can be measured using spectrophotometry.

Fluorometric assays [26] involve using fluorescent probes that selectively react with H₂O₂, generating a fluorescent signal that can be quantified with a fluorometer. A widely used fluorometric probe is 2',7'-dichlorofluorescein diacetate (DCFH-DA), which is converted to the fluorescent compound DCF upon reaction with H₂O₂ [27].

Spectrophotometric assays employ spectrophotometry to measure the absorption of a colored product resulting from the reaction between H₂O₂ and a specific substrate. Guaiacol is a typical substrate used in this method, reacting with H₂O₂ in the presence of peroxidase to produce a brown color that can be measured using spectrophotometry [28,29].

Electrochemical methods involve the use of electrodes capable of detecting changes in H₂O₂ concentration. Amperometric and potentiometric electrodes are commonly used to measure H₂O₂ concentration in plant tissues [30–32].

Overall, the choice of method for H₂O₂ determination in plants depends on factors such as the sensitivity, specificity, and cost of the method, as well as the specific research question being addressed.

Electrochemical methods provide several advantages compared to other approaches for quantifying H₂O₂ concentration in plants. Electrochemical sensors demonstrate high sensitivity and are capable of detecting low H₂O₂ concentrations in the nanomolar or micromolar range [33,34]. Electrochemical methods allow for the real-time, non-destructive measurement of H₂O₂ levels in plant tissues [10]. Electrochemical methods exhibit high selectivity for H₂O₂, enabling researchers to measure H₂O₂ concentrations in the presence of other ROS or interfering compounds. Electrochemical sensors can be miniaturized and integrated into portable devices, making them suitable for on-site or field-based measurements of H₂O₂ in plants [35]. Furthermore, electrochemical sensors are cost-effective compared to other analytical methods, making them accessible to researchers with limited budgets and allowing for mass production.

Both enzymatic and non-enzymatic electrochemical sensors are utilized for H₂O₂ detection.

Enzymatic sensors employ the enzyme horseradish peroxidase (HRP) to catalyze the reduction of H_2O_2 [36–38]. This reaction generates an electrical current proportional to the H_2O_2 concentration in the sample. Enzymatic sensors offer high selectivity for H_2O_2 and can detect nanomolar concentrations. However, due to the inherent instability of enzymes, such electrodes are susceptible to temperature and environmental influences and can be easily damaged.

Non-enzymatic sensors, on the other hand, utilize materials such as metal oxides [39,40], carbon materials [41], or conducting polymers [42] that exhibit sensitivity to H_2O_2 . Non-enzymatic sensors operate based on a direct chemical reaction between the analyte and the electrode material's surface. Manufacturing non-enzymatic sensors is more cost-effective, and they tend to be more stable and have a longer lifespan compared to enzymatic sensors. However, they may exhibit slightly lower sensitivity than enzyme sensors. To enhance the sensitivity of non-enzymatic sensors, smooth-film coatings can be replaced with nanostructured ones. Nanostructures increase the surface area of the working electrode, providing more reactive sites for H_2O_2 interaction [43,44]. Additionally, nanostructures can facilitate the electron transport between the sensor and H_2O_2 molecules, thereby improving detection accuracy and speed.

Some of the most common materials used for detecting hydrogen peroxide are metal oxides (CuO , Co_3O_4 , TiO_2 , etc.) [45,46]. When H_2O_2 comes into contact with metal-oxide nanostructures, several processes can occur [46,47]. During the adsorption process, H_2O_2 molecules are adsorbed onto the surface of metal-oxide nanostructures through hydrogen bonding or other interactions, which can affect the concentration and reactivity of H_2O_2 . The adsorption process can be influenced by the surface charge and functional groups of the nanostructures. Also, along with other processes, electron transfer reactions take place: metal-oxide nanostructures undergo electron transfer with H_2O_2 , leading to the generation of reactive oxygen species such as hydroxyl radicals ($\bullet\text{OH}$). This process is known as the Fenton reaction [48] and can be enhanced by the presence of transition metal ions such as iron or copper. The second process is catalytic decomposition, where metal-oxide nanostructures act as catalysts for the breakdown of H_2O_2 into water and oxygen. The high surface area and active sites of the nanostructures accelerates this reaction.

Overall, the interaction between metal-oxide nanostructures and H_2O_2 can lead to changes in the electrical properties of the metal oxide surface, which can be measured by an electrochemical sensor to detect the presence and concentration of H_2O_2 .

To enhance the performance of electrochemical sensors, a multisensor system can be employed, utilizing multiple electrodes modified with electroactive materials [49,50]. Incorporating multiple electrodes expands the possibilities for signal modeling, significantly enhances measurement accuracy, and provides additional information about the composition of the solution due to cross sensitivity and complementary electroactive properties of the electrodes made from different materials. This approach can improve sensor selectivity for the analyzed analyte and enable the detection of trace amounts. Moreover, a multisensor system enables the simultaneous detection of multiple analytes, which is crucial for monitoring complex compositions and tracing the concentration dependence of one component on another.

The purpose of this article is to study the influence of various stress factors on the growth and vital functions of rye seedlings and also to develop an electrochemical sensor based on nanostructured CuO and Co_3O_4 electrodes, which makes it possible to determine the amount of H_2O_2 released in plant tissues under the influence of oxidative stress in real samples of rye juice.

2. Materials and Methods

2.1. Materials

Ammonium persulfate ($(\text{NH}_4)_2\text{S}_2\text{O}_8$, CAS number: 7727-54-0), sodium hydroxide (NaOH , CAS number: 1310-73-2), cobalt(II) chloride hexahydrate, ($\text{CoCl}_2 \cdot 6\text{H}_2\text{O}$, CAS number: 7791-13-1), urea NH_2CONH_2 (CAS number: 57-13-6), sodium chloride (NaCl , CAS

number: 7647-14-5), potassium nitrate (KNO_3 , CAS number: 7757-79-1), glucose ($\text{C}_6\text{H}_{12}\text{O}_6$, CAS number: 50-99-7) citric acid ($\text{HOC}(\text{COOH})(\text{CH}_2\text{COOH})_2$, CAS number: 77-92-9), ascorbic acid ($\text{C}_6\text{H}_8\text{O}_6$ CAS number: 50-81-7), and hydrogen peroxide solution (H_2O_2 , 30%, CAS number: 7722-84-1) were purchased from Merck. All reagents were $\geq 99.8\%$ pure. Copper and iron wires of 2 mm thickness (99.9% purity) were purchased from Sigma-Aldrich. Ag/AgCl wire was purchased from A-M Systems, USA. Carbon rods (5 mm diameter) were purchased from Sigma-Aldrich. Rye seeds (*Secale Cereale* L. TORAF, batch PL81604335/27TDC/1) were purchased from a local store. Distilled water was obtained in the laboratory.

2.2. Synthesis of Nanostructured Samples

Electrodes coated with nanostructured CuO were obtained by a one-step chemical hydrothermal oxidation route. To accomplish this, copper wire was cut into 6 cm long pieces and thoroughly rinsed with both water and ethanol to eliminate any potential surface contamination. Subsequently, the cleaned wire segments were vertically affixed onto the surface of a petri dish using heat-resistant foam. To prepare the working solution, 10 mL of a 10 M NaOH solution and 5 mL of a 1 M $(\text{NH}_4)_2\text{S}_2\text{O}_8$ solution were combined with 26 mL of distilled water. The resulting solution was transferred into a heat-resistant glass beaker, and the wire samples were immersed in the solution. The petri dish was used to cover the beaker. The beaker, containing the solution and wire samples, was placed inside a preheated oven set at 90 °C for 3 h, followed by natural cooling. Afterward, the obtained samples, now coated with a nanostructured oxide layer, were thoroughly rinsed with distilled water to eliminate any residual reagents. Finally, they were dried in an oven at 90 °C for 3 h to remove any remaining moisture. To minimize environmental effects, the samples were stored in a vacuum desiccator until the moment of use. The synthesis process was described in more detail in publication [51].

Electrodes coated with nanostructured Co_3O_4 were obtained using a hydrothermal synthesis method. Iron wire was used as a base for the nanostructured layer. Before the synthesis of the coating, the wire was treated with fine sandpaper and immersed in 0.1 M HCl to increase the roughness of the electrode surface and improve the adhesion of the nanostructures. The wire was then cut into 6 cm long pieces, rinsed with water and ethanol, and fixed in a glass beaker following the same procedure as the CuO samples mentioned above. For the synthesis, an equimolar aqueous solution of 0.1 M $\text{CoCl}_2 \cdot 6\text{H}_2\text{O}$ and NH_2CONH_2 was mixed in 80 mL of distilled water to form a growth solution. The solution was poured into glass beaker, and the pre-treated iron wire was placed in the beaker. The beaker with the solution and wire was then placed in a preheated oven. The growth of nanostructures took place 5 h at 95 °C, resulting in a dull pink $\text{Co}(\text{OH})_2$ coating. After cooling to room temperature, the wire electrodes were washed with distilled water several times to remove residual reagents and then dried at 90 °C for 3 h. Subsequently, the growth process was followed by thermal decomposition of $\text{Co}(\text{OH})_2$ for 1 h at 450 °C to obtain Co_3O_4 . After annealing, a black and homogeneous Co_3O_4 coating was observed on the surface of the wire electrodes. The morphology of the CuO and Co_3O_4 nanostructures was studied by the Field Emission Scanning Electron Microscopy (FESEM) MAIA3 (Tescan Group, Brno-Kohoutovice, Czech Republic).

2.3. Rye Seedling Cultivation and Sample Preparation

To investigate the impact of stress factors, the samples were divided into four groups, with each group containing four containers: control, NaCl-treated, glyphosate-treated, and H_2O_2 -treated. The seed germination process utilized a universal soil for indoor plants, and all samples were subjected to the same growth conditions, except for the composition of the watering solution.

During the seed germination and initial growth stages, all samples received a daily watering of 20 mL of deionized water per container for a period of 10 days. From day 11 onwards, the control group continued to receive 20 mL of water daily, while the other

groups were watered with 20 mL of a 100 mM NaCl solution, 20 mL of a 100 μ L/50 mL glyphosate solution, and 20 mL of a 1.5% H₂O₂ solution, respectively. This watering regimen was maintained for an additional 10 days. At the end of the 10-day period, morphological differences among the samples were assessed through control measurements. On day 11, rye samples were harvested to obtain an extract. The leaves were cut into small pieces, crushed using a mortar and pestle, and then placed in 96% ethanol for spectrometric measurements or NaOH supporting electrolyte for electrochemical measurements. For optical measurements, 250 mg of green mass per 5 mL of alcohol was used, while for electrochemical measurements, 10 g of green mass per 250 mL of supporting electrolyte was employed. The samples were left overnight in a cool, dark place to facilitate extraction. Prior to measurement, the solutions were filtered to remove solid particles.

2.4. Optical Measurements

The amount of chlorophyll is one of the most important indicators of plant life, and its decrease is an important indicator for assessing the impact of stress factors. In this study, the chlorophyll content of photosystem II (PSII) and photosystem I (PSI) were analyzed by extracting chlorophyll from leaves of rye seedlings that were either untreated or treated with different stress factors.

To perform the analysis, a working solution was prepared as described in the previous section and poured into a 5 mL transparent cuvette for measurement. Five replicates were performed for each treatment group. The samples were analyzed using a UV-Visible two-beam spectrophotometer SHIMADZU UV-2550PC (Shimadzu Corporation, Kyoto, Japan). The absorbance of each treatment sample was measured at wavelengths of 645 and 663 nm to determine the quantities of chlorophyll *a* and *b*, respectively. The measurement error was less than 2%. The estimation of chlorophyll content was conducted utilizing Arnon's Equations (1) and (2) [52–54]:

$$\text{Chla (mg/g)} = [12.7 \times A_{663} - 2.69 \times A_{645}] \times V/1000 \times W \quad (1)$$

$$\text{Chlb (mg/g)} = [22.9 \times A_{645} - 4.86 \times A_{663}] \times V/1000 \times W \quad (2)$$

where V—volume of the extract in mL; W—weight of fresh leaves in mg; A₆₆₃—solution absorbance at 663 nm; and A₆₄₅—solution absorbance at 645 nm.

2.5. Electrochemical Measurements

The measurements were carried out using a custom device that allowed simultaneous measurements and data acquisition from two working electrodes with different chemical composition. To validate the accuracy of the setup, electrochemical measurements under absolutely identical conditions were carried out separately for each oxide using an electrochemical station Zahner Zennium X (Zahner-Elektrok GmbH & Co., Kronach, Germany). During the measurement, a three-electrode cell configuration was adopted. The working electrodes consisted of the nanostructure-coated wires. Additionally, a 2 mm diameter Ag/AgCl wire was employed as the reference electrode, while a 5 mm diameter carbon rod served as the counter electrode.

Cyclic voltammetry (CV) was performed within specific voltage ranges for each electrode. For the Co₃O₄ nanostructured electrode, the voltage range was set from -1.3 V to 0.5 V vs. Ag/AgCl, with $E_{\text{start}} = 0$ V and a scan rate of $100 \text{ mV} \cdot \text{s}^{-1}$. For the CuO electrode, the voltage range was -0.8 V to 0.1 V vs. Ag/AgCl, with $E_{\text{start}} = 0$ V and a scan rate of $100 \text{ mV} \cdot \text{s}^{-1}$. The supporting electrolyte used was 0.1 M NaOH , providing an optimal pH level of 13.

To assess the sensitivity of the electrodes, different concentrations of H₂O₂ ranging from $25 \mu\text{M}$ to 5 mM were added to the supporting electrolyte.

In the current response study, a constant voltage was applied to the cell, and the resulting current was measured. Precisely, a constant voltage of $U = -1.23$ V vs. Ag/AgCl was applied to the cell for the Co₃O₄-nanostructured electrode, and a constant voltage

of $U = -0.7$ V vs. Ag/AgCl was applied for the CuO electrode. These potential values were taken from the left reduction peaks from CV graphs obtained at a scanning speed of 100 mV/s. The measurements were conducted in 0.1 M NaOH supporting electrolyte. The measurements were started in the supporting electrolyte without hydrogen peroxide, and after a stabilization period of 120 s, the first 25 μ M portion of H_2O_2 was added. Subsequent portions were added every 120 s. The measurements were conducted with constant stirring using a magnetic stirrer in a water bath at a constant temperature of 25 $^{\circ}$ C.

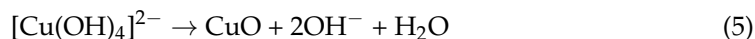
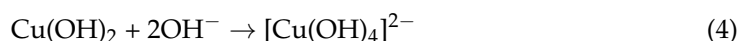
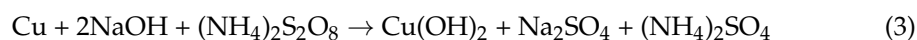
To obtain a calibration curve, H_2O_2 concentrations from 25 μ M to 7 mM were added. Interference studies were also conducted to ensure that there were no false-positive enhancements in the electrochemical response caused by interfering substances. To assess this, 100 μ M portions of the most likely interferents, such as NaCl, KNO_3 , glucose, citric acid, and ascorbic acid, were added to the supporting electrolyte. In the process of testing the sensor, we used different ratios of H_2O_2 and interferents (including cases where the concentration of the interferent notably exceeded the concentration of the analyte). Since in the process it was found that the ratio between the concentrations of the analyte and interferents did not affect the result obtained, we decided to adhere to an equimolar ratio, as in most similar publications. In the study of real samples, a NaOH-based extract was used.

Since the amount of H_2O_2 released under the influence of stress factors is unknown, during the measurement process, a number of known concentrations were added to the extract and the chronoamperogram was taken. After the necessary calculations with reference to the calibration graph were obtained for the supporting electrolyte, the concentration of the found H_2O_2 was calculated. The amount of H_2O_2 released in the plants as a result of exposure to stress factors was taken to be the difference between the total amount of peroxide found and that added artificially during the measurement process.

The infusion of peroxide took place at a strictly defined time, and the current value was calculated as the average of the points on the chronoamperogram over a certain period of time. To obtain data on the found amount of peroxide indicated in Results and Discussion section, averaged data based on several batches of samples were used.

3. Results and Discussion

Figure 1a–c display the results of the FESEM analysis, showing the morphology of the CuO layer obtained through chemical hydrothermal oxidation. The black coating exhibited excellent uniformity (Figure 1a), strong adhesion to the copper surface, and stability during post-processing. It consisted of a dense layer of nanopetals that were clustered together in 3D flower-like structures with a micrometer size (Figure 1b,c). The growth mechanism of the nanostructures followed a series of chemical reactions outlined by Equations (3)–(5):



The addition of NaOH to the precursor solution containing $(NH_4)_2S_2O_8$ released Cu^{2+} ions from the copper, which interacted with the reagents according to Equation (3). However, when the concentration of NaOH was increased to 10–15 mM, the dissolution-secondary precipitation mechanism was activated. In this process, $Cu(OH)_2$ reacted with OH^- ions, forming the complex ion $[Cu(OH)_4]^{2-}$ as illustrated in Equation (4). These complex ions decomposed to CuO, resulting in the loss of two hydroxyl ions and one water molecule, as depicted in Equation (5).

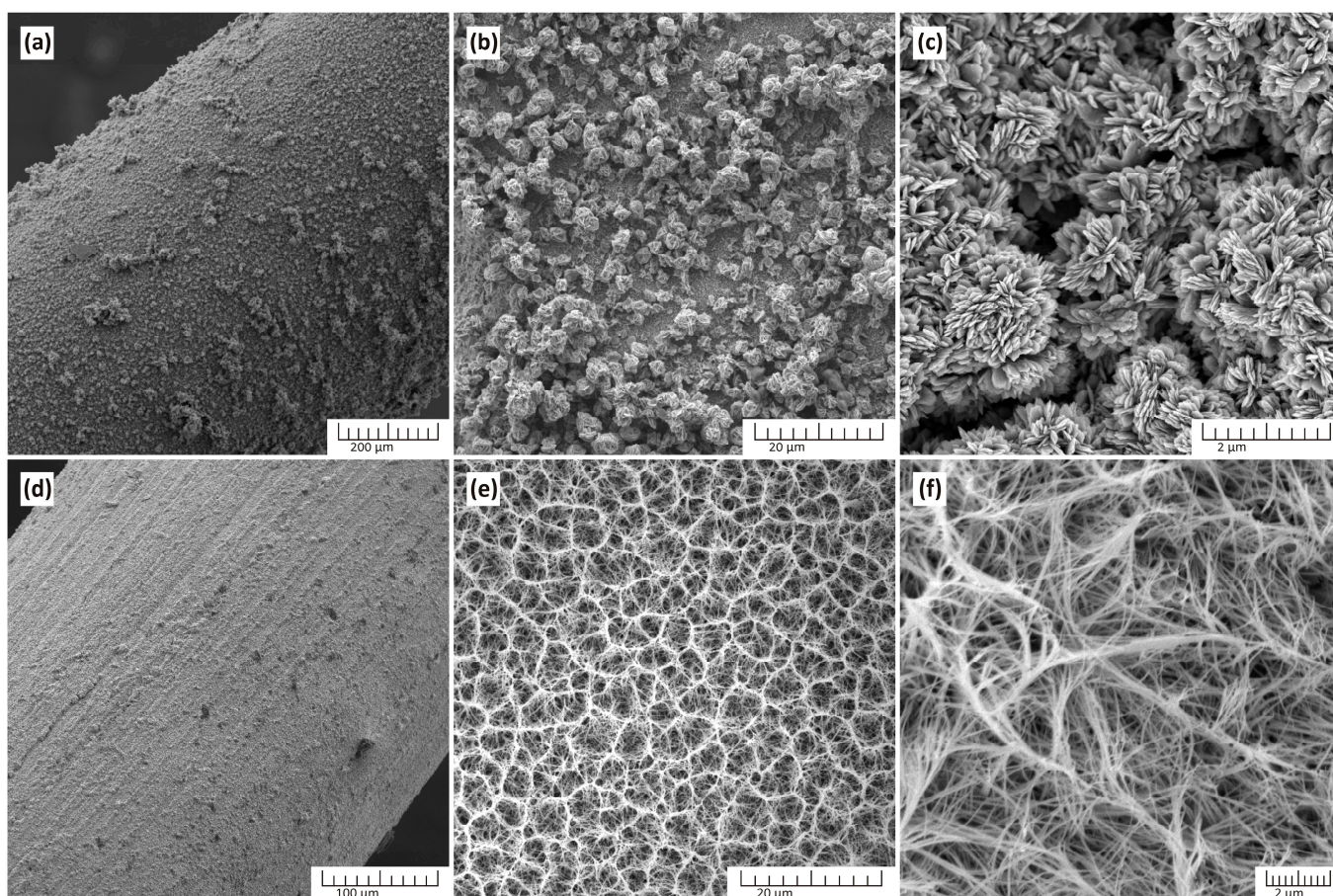
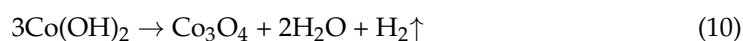
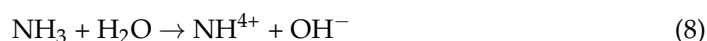
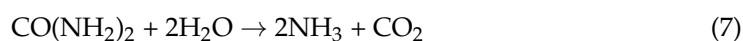


Figure 1. FESEM images of wire samples with CuO and Co₃O₄ nanostructures at different magnifications. The top row (a–c) shows the CuO nanostructures. Image (a) reveals a general view of a wire electrode with nanostructured CuO layer, while images (b,c) display a nanostructured CuO layer at increasing magnifications. The bottom row (d–f) depicts the Co₃O₄ nanostructures. Image (d) illustrates a general view of a wire electrode with a nanostructured Co₃O₄ layer, images (e,f) presents a honeycomb-like Co₃O₄ nanostructured surface at increasing magnifications. The scale bars in each image indicate the level of magnification.

SEM images of the Co₃O₄ nanostructures are presented in Figure 1d–f, revealing a uniform and porous network of long nanofibers covering the wire surface.

The typical reactions involved in the formation of the nanoporous Co₃O₄ nanostructure are summarized as follows:



The growth process included the hydrothermal synthesis of cobalt hydroxide (Equations (6)–(9)) and its thermal decomposition to cobalt oxide (Equation (10)).

Figure 2 shows X-ray diffraction patterns of the obtained nanostructures. The patterns indicated the presence of only crystalline phases corresponding to CuO and Co₃O₄, confirming their high purity. No inclusions with other chemical compositions were observed. The samples exhibited a relatively high degree of crystallinity, although the intensity of

characteristic peaks for Co_3O_4 was lower compared to CuO . This was probably due to the fine fibrous porous structure of the Co_3O_4 sample and to the peculiarities of the growth process and the fact that the copper oxide used the substrate material itself rather than the solution as a precursor source.

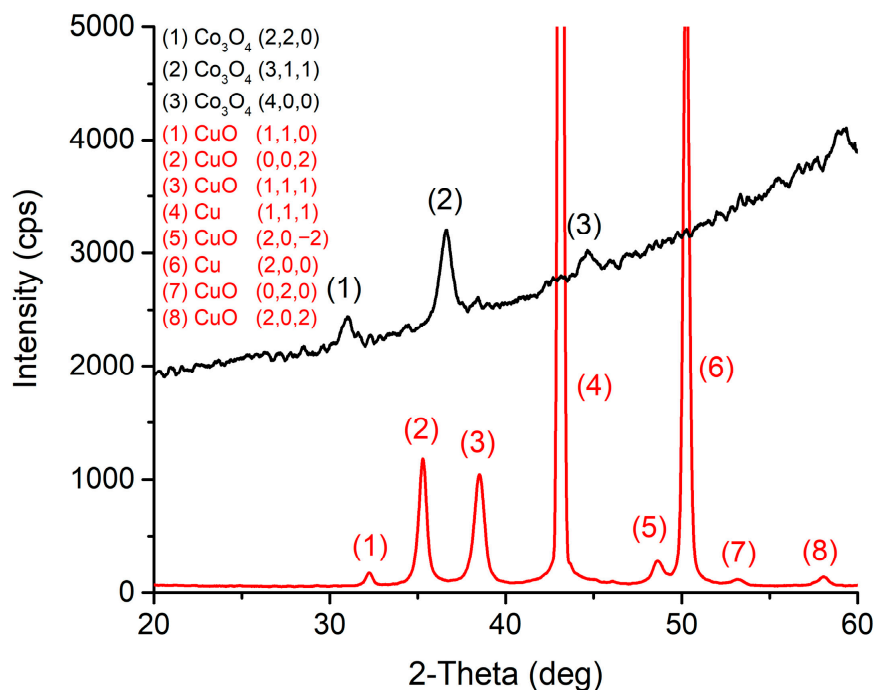


Figure 2. XRD patterns of obtained nanostructures.

Figure 3 shows the rye samples at the time of cutting, arranged from left to right: control, NaCl -treated, H_2O_2 -treated, and glyphosate-treated. After cutting and measuring the length of the seedlings, the following trend was observed: the control sample exhibited the longest seedling length (average 20 cm, maximum 23 cm), followed by the peroxide-treated sample (average 19 cm, maximum 23 cm), the NaCl -treated sample (average 17 cm, maximum 19 cm), and the glyphosate-treated sample with the shortest length (average 16 cm, maximum 19 cm). Furthermore, in the NaCl - and glyphosate-treated samples, an increased presence of mold was observed on the soil surface, indicating a suppression of plant resistance to fungal diseases under the influence of stress factors.

In Figure 4, the absorption spectra of rye extracts are presented. It is noteworthy that the concentration of chlorophyll in the freshly prepared samples appeared to be higher in the case of H_2O_2 watering, even surpassing the control sample. This finding demonstrates that the addition of small concentrations of H_2O_2 to irrigation not only does not harm plants but actually has a positive impact. It can stimulate root growth, enhance nutrient absorption, and improve overall plant growth and development. H_2O_2 can assist in breaking down organic matter in the soil, thereby releasing essential nutrients needed for plant growth.

In contrast, the plants watered with glyphosate and NaCl exhibited a significantly lower concentration of chlorophyll *a* and chlorophyll *b* compared to the control samples. This observation suggests that plant vital functions decrease significantly under the influence of these stress factors. It is important to note that the effect of NaCl was comparable to that of glyphosate, a potent herbicide, confirming the harmful impact of increased soil salinity. After storing the samples in a dark and cold environment for a week, all the samples demonstrated a reduction in transmission, indicating a general decrease in chlorophyll concentration. However, there was a noticeable difference between the transmission of the watered samples with H_2O_2 and the control samples. Unlike the previous case where their peaks almost coincided, this suggests a slower process of chlorophyll decomposition in the H_2O_2 -watered samples compared to the control samples. Regarding the watered samples

with NaCl and glyphosate, the absorption peaks for chlorophyll *a* were practically the same. For chlorophyll *b*, there was a difference with an increase towards NaCl. The concentration of chlorophyll was calculated according to Equation 1 and 2, and the obtained data are summarized in Table 1.



Figure 3. Samples of rye on the day of collection of green mass for further research. From left to right: control, treated with NaCl, H₂O₂, and glyphosate.

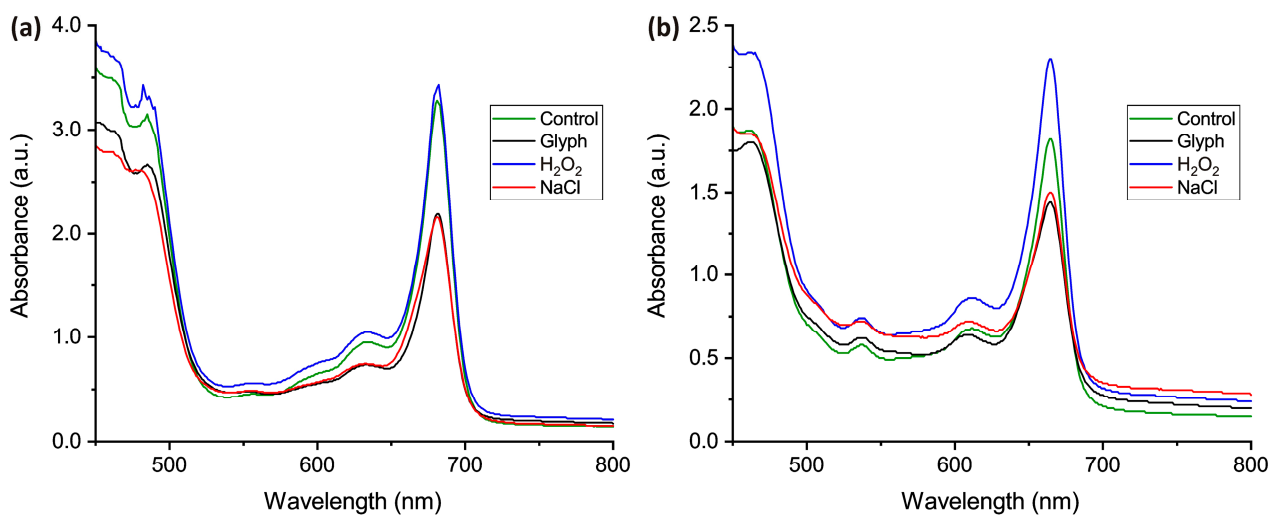


Figure 4. Absorbance measurement for as-prepared samples (a) and samples stored in cool dark place for 1 week (b).

Table 1. Changes in chlorophyll concentration in rye samples grown under the influence of different stress factors.

Stress Factor	As Prepared Samples		After 1 Week of Storage	
	Chl(<i>a</i>), (mg/g)	Chl(<i>b</i>), (mg/g)	Chl(<i>a</i>), (mg/g)	Chl(<i>b</i>), (mg/g)
H ₂ O ₂	47.80	19.27	32.61	18.62
Control	45.88	17.82	25.45	14.73
Glyphosate	31.39	14.40	21.00	15.82
NaCl	30.10	19.21	19.79	16.07

Table 1 presents notable variations in the chlorophyll concentration, particularly in chlorophyll *a*. Upon analyzing the samples on the day of collection, the following relative changes were observed compared to the control: a decrease of 31.5% in the samples cultivated with NaCl, a decrease of 34.7% in the samples subjected to glyphosate, and a slight increase of 2.2% in the samples treated with hydrogen peroxide. After storing the samples in a dark and cool environment for a week and conducting repeated measurements, the corresponding values were obtained: a reduction in the concentration to 22.2% and 17.5% for the NaCl and glyphosate samples, respectively, and an increase of 28.1% in the H₂O₂-treated samples compared to the reference sample. These findings indicate that the decomposition of chlorophyll in the samples irrigated with water containing low concentrations of H₂O₂ significantly slowed down over time compared to the reference sample.

Figure 5 shows CV graphs for the CuO and Co₃O₄ electrodes performed in a 0.1 M NaOH supporting electrolyte to determine the electrochemical response of the electrodes to the addition of various H₂O₂ concentrations.

In previous studies, it was observed that for effective catalytic processes between H₂O₂ and CuO and Co₃O₄ nanostructures, an alkaline medium is necessary, with the best electrochemical response occurring at pH = 12.5–13 [51]. This pH range can be achieved by using a 0.1 M solution of NaOH or KOH. According to the literature, this phenomenon is attributed to the generation of OH[−] ions from oxyhydroxide products, which diffuse into the nanostructured layer and enhance its conductivity compared to hydroxide ions. As a result, there is an increased driving potential towards the wire substrate, enabling the successful detection of H₂O₂ when a negative applied potential activates the Co₃O₄ electrode in an alkaline solution. The CV curves obtained for different pH levels of the supporting electrolyte are shown in Figure 5, where Figure 5c shows the results for the nanostructured CuO electrode and Figure 5d displays the results obtained for the Co₃O₄ nanostructured electrode.

Furthermore, it was determined that the scan rate significantly influenced the height of the oxidation and reduction peaks observed in CV graphs. It was found that the optimal scan rate was 100 mV/s. Increasing the scan rate beyond this value did not lead to a significant increase in the peak height, and in some cases, it even reduced the peak height. Therefore, a scan rate of 100 mV·s^{−1} was determined to be the optimal parameter for the electrochemical measurements. Changes in the CV curves depending on the scanning speed are shown in Figure 5e for the CuO electrode and in Figure 5f for the Co₃O₄ electrode.

The CV graph of CuO (Figure 5a) revealed the presence of two pairs of peaks representing the transitions from Cu⁰/Cu⁺ and Cu⁺/Cu²⁺ during the oxidation process. Additionally, there were a pair of reduction peaks indicating the Cu²⁺/Cu⁺ and Cu⁺/Cu⁰ transitions.

The Co₃O₄-modified electrode displayed two distinct pairs of well-defined redox peaks (Figure 5b). The reversible transition between Co₃O₄ and CoOOH can be attributed to one pair of redox peaks, while the further conversion between CoOOH and CoO₂ can be associated with another pair of redox peaks.

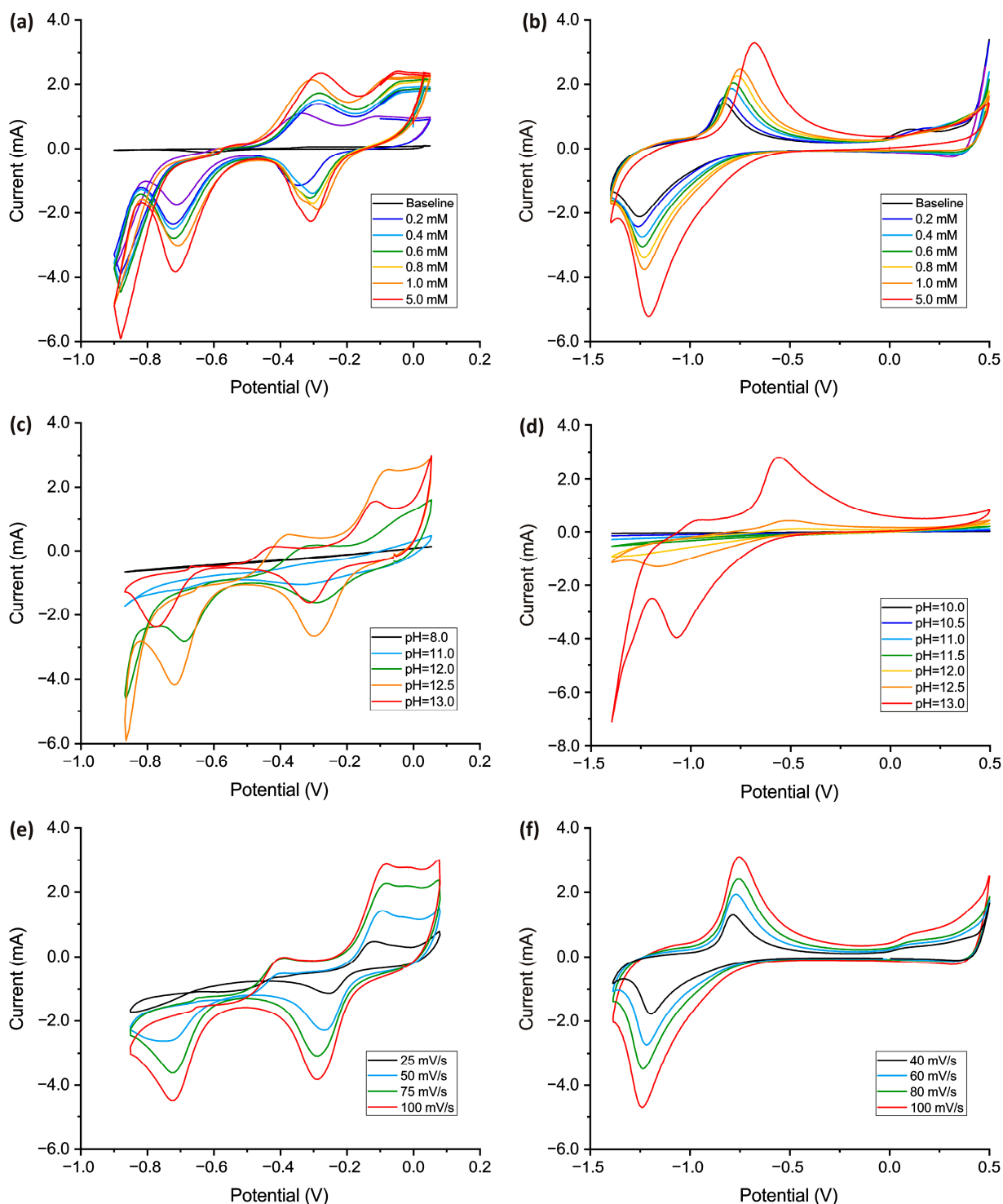


Figure 5. CV graph of nanostructured CuO and Co₃O₄ electrodes obtained in a supporting electrolyte solution and in solutions containing various concentrations of H₂O₂. The measurements were carried out in NaOH supporting electrolyte (pH = 13) at a scanning rate of 100 mV·s⁻¹. Here, (a) is data for the electrode coated with CuO nanostructures and (b) is data obtained for the Co₃O₄ electrode. Comparison of CV curves obtained at different pH values of supporting electrolyte containing 5 mM H₂O₂, where (c) is data for CuO electrode and (d) is data for Co₃O₄ electrode. Comparison of CV curves obtained at different scan speeds. Measurements were carried out in 0.1 M NaOH solution containing 5 mM H₂O₂, where (e) is data for CuO electrode and (f) is data for Co₃O₄ electrode.

The catalytic reactivity of both oxides was prominently observed upon the introduction of H_2O_2 into the solution, leading to a noticeable amplification in the peaks associated with oxidation and reduction processes on the CV graphs. Remarkably, even at low analyte concentrations, these peaks exhibited substantial enhancement, underscoring the high sensitivity exhibited by these materials.

The electron transfer mechanism at the modified CuO electrode can be described as follows: In this catalytic process, when H_2O_2 was reduced on the CuO surface, Cu^{2+} was electrochemically reduced to Cu^+ while H_2O_2 was transformed into O_2 . Subsequently, the Cu^+ on the electrode surface underwent electrooxidation back to Cu^{2+} , initiating a repeated catalytic cycle.

In the case of the nanostructured Co_3O_4 electrode, the cobalt oxide acted as a catalyst, facilitating the decomposition of H_2O_2 into CoOOH and H_2O . The Co_3O_4 surface provided active sites where the oxidation of H_2O_2 took place, leading to the formation of CoOOH .

Figure 6 presents the chronoamperograms of the nanostructured CuO electrode (Figure 6a) and the nanostructured Co_3O_4 electrode (Figure 6b) upon the introduction of H_2O_2 at concentrations ranging from 20 μM to 7 mM. Both oxides exhibited a distinct and well-defined step in the plot upon the addition of even low concentrations of hydrogen peroxide, demonstrating the high sensitivity of the sensor and a clear response to the target analyte. Notably, the step quickly reached a plateau, indicating a rapid response and prompt stabilization of the electrode upon the introduction of the analyte. The calibration curve shows that both oxides exhibited a good linear dependence over the entire concentration range from 20 μM to 7 mM, which indicates that the sensors based on these structures could equally successfully be used to determine both low and relatively high concentrations of the analyte.

The sensitivity of the obtained CuO electrode was $439.19 \mu\text{A}\cdot\text{mM}^{-1}$, and the calculated LOD was 1.34 μM , assuming a signal-to-noise ratio of 3. The sensitivity of Co_3O_4 electrode was $505.11 \mu\text{A}\cdot\text{mM}^{-1}$, and, considering a signal-to-noise ratio of 3, the calculated LOD was found to be 1.05 μM .

Figure 6c,d show the chronoamperograms of the addition of 50 μM and 100 μM H_2O_2 in real rye juice samples for the CuO electrode (Figure 6c) and the Co_3O_4 electrode (Figure 6d). The curves obtained from the real samples exhibited lower stability compared to the similar curves generated in a supporting electrolyte with prescribed concentrations of hydrogen peroxide, which were used to construct the calibration graph. This disparity was likely attributed to the complexity of the plant juice as an analyte, which comprised a diverse matrix containing numerous organic and inorganic compounds, as well as solid plant tissue components. While these components may not have functioned as interferents, they appeared to have a detrimental impact on the system's stability. To address this issue, we employed the methodology described in the Section 2. We saw that despite the complex chemical composition of the analyzed solution, there was a fast and accurate electrochemical response to the addition of a portion of H_2O_2 . This proves the possibility of the successful application of this sensor for the further implementation of the spike method for detecting low concentrations of H_2O_2 in these samples.

The dynamics of these graphs should be highlighted, as they reveal important insights. Notably, the control sample, which was not subjected to any stress factors during growth, exhibited the lowest electrochemical response. Following that, the sample exposed to low concentrations of H_2O_2 showed a slightly higher response. Remarkably, a significant margin separated the electrochemical response of the sample grown under salt stress, and even more pronounced was the response obtained for the plants grown under the influence of glyphosate. The response corresponding to salt stress closely resembled the response observed in plants exposed to herbicides. This dynamic trend was observed in both the CuO and Co_3O_4 electrodes.

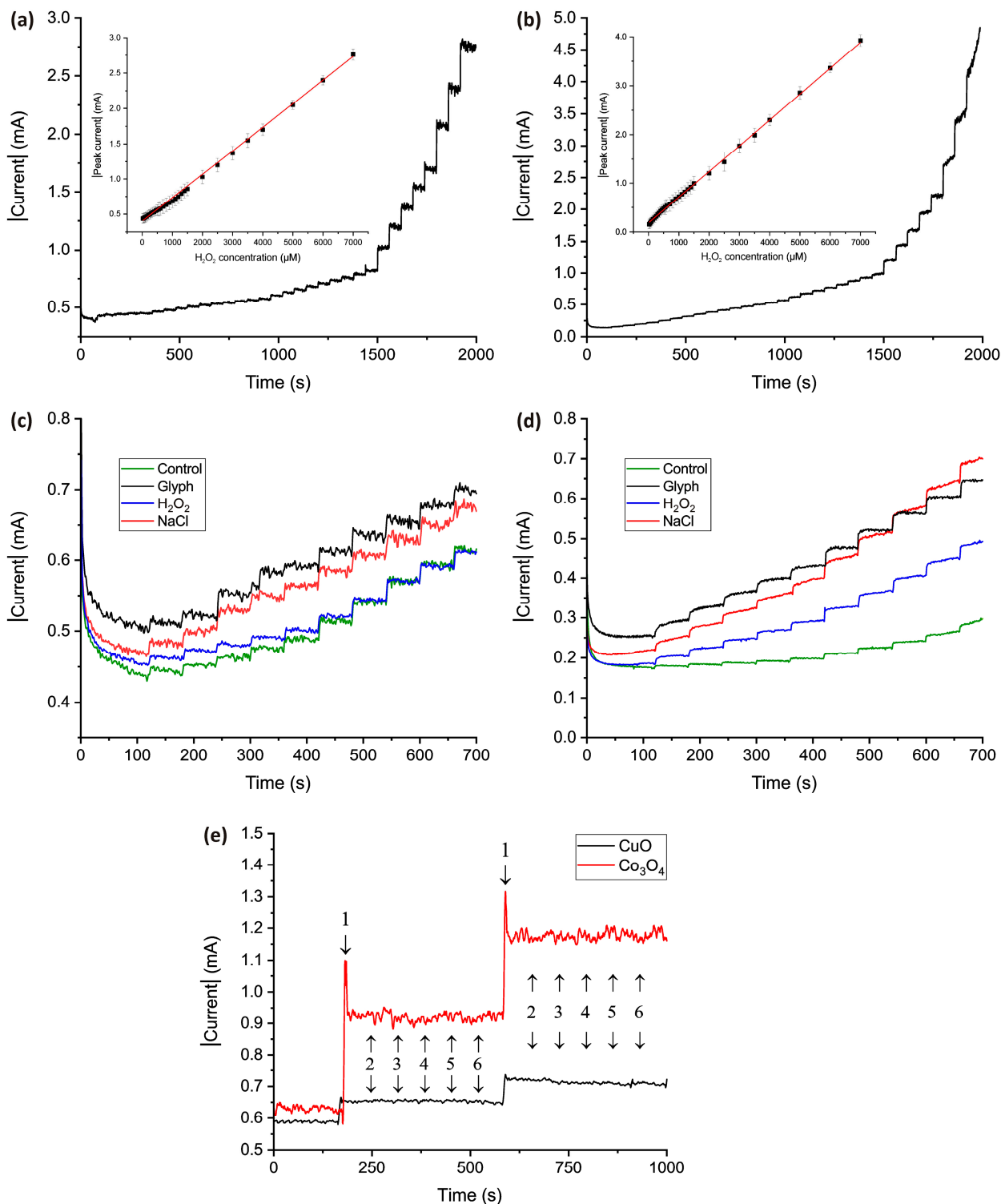


Figure 6. Chronoamperograms in a supporting electrolyte for (a) CuO and (b) Co₃O₄ nanostructured electrode for -0.7 V and at -1.23 V peak potentials obtained by adding H₂O₂ in the concentration range from 20 μ M to 7 mM. Inset: the corresponding calibration concentration dependence. Chronoamperograms in real samples of rye juice obtained by adding a H₂O₂ in the concentration range from 50 μ M to 750 μ M for (c) CuO nanostructured electrode and (d) Co₃O₄ nanostructured electrode. (e) Interference study with the addition of H₂O₂ (1) and potential interfering substances NaCl (2), KNO₃ (3), glucose (4), citric acid (5), and ascorbic acid (6).

Figure 6c,d show that both electrodes exhibited a consistent trend reflecting the H_2O_2 content, with the samples arranged in the following increasing order of released hydrogen peroxide: control, H_2O_2 , NaCl, and glyphosate. However, it is worth noting that the Co_3O_4 electrode consistently displayed a higher electrochemical response across all samples compared to the CuO electrode. This discrepancy may, in part, be attributed to our approach, where we utilized results obtained from multiple batches of plant samples and calculated the average value. It is also worth noting that this phenomenon was exclusively observed in the rye samples subjected to stress, where a substantial amount of H_2O_2 was evidently released. The results obtained from both sensors on the control samples in this article, as well as the test measurements in the buffer solution and even the real milk samples described in our previous articles, aligned closely for both electrodes and matched the reference values on the calibration line. This led us to assume that under stress conditions, the plants released a specific substance, potentially another type of ROS, which reacted with the surface of the Co_3O_4 electrode, resulting in a false increase in the electrochemical response, while not eliciting a similar reaction with CuO.

Considering that a plant is an intricate chemical system with a complex composition, further investigation is needed to define this substance accurately. Nevertheless, this phenomenon can be further leveraged positively in the development of a multisensory system, where differences between signals obtained from CuO and Co_3O_4 electrodes can be analyzed mathematically and utilized as one of the parameters for determining H_2O_2 concentration in plants.

As mentioned earlier, plant juice is a matrix consisting of various components such as solid cellular structures, organic acids, sugars, and more. Therefore, when developing an electrochemical sensor to work with such analytes, it is crucial to eliminate the possibility of false increases in the electrochemical response caused by interfering substances. In order to achieve this, both electrodes underwent testing for interferences by introducing substances like NaCl, KNO_3 , glucose, citric acid, and ascorbic acid, along with H_2O_2 . Figure 6e demonstrates that both electrodes exhibited excellent selectivity, as an electrochemical response was only observed when a $100\ \mu\text{M}$ portion of H_2O_2 was introduced into the solution. The addition of interferents at the same concentration did not induce any change in the current higher than the level of noise.

To analyze the content of hydrogen peroxide in real samples using nanostructured CuO and Co_3O_4 electrodes, a recovery test was conducted, and the results are presented in Table 2.

Here, the “added” column corresponds to the concentration of peroxide added to the sample during measurement, the “found” column corresponds to the total amount of H_2O_2 detected by the sensor, and the “excess” column corresponds to the amount of H_2O_2 that was released by the plant under the influence of stress factors.

It can be seen that in the case of both oxides for the baseline, the recovery practically coincided, and the amount of extra found H_2O_2 corresponding to the released peroxide was close to 0, which indicates the accurate operation of the sensor and the absence of additional hydrogen peroxide in the control sample.

In the case of the samples treated with H_2O_2 watering, in a number of spike concentrations, an excess of 100% was observed for both oxides, while the average amount of released H_2O_2 was $38.5\ \mu\text{M}$ for CuO and $26.5\ \mu\text{M}$ for Co_3O_4 .

Much more significant changes were observed when the plants were exposed to salt and herbicide stress during growth. So, for NaCl, the average amount of excess H_2O_2 was determined as $113.6\ \mu\text{M}$ in the case of CuO and $133.2\ \mu\text{M}$ in the case of Co_3O_4 . For the glyphosate-treated samples, the average amount of excess H_2O_2 was determined to be $163.02\ \mu\text{M}$ for CuO and $223.03\ \mu\text{M}$ for Co_3O_4 .

The data obtained clearly indicate that a significant amount of H_2O_2 was released in the rye samples under the influence of salt stress and herbicide stress. Moreover, in terms of the amount of a certain peroxide, the effect of NaCl was just as detrimental to the plant as the effect of glyphosate, which, by definition, has a herbicidal (depressant) effect. This

fact additionally confirms the damage caused to plants by increased soil salinity caused by technogenic factors and a deliberate neglect of the norms of recommended concentrations of applied fertilizers.

Table 2. Study of the increase in the content of H₂O₂ in rye samples grown under the influence of various stress factors.

CuO							
Control				H ₂ O ₂			
Added (μM)	Found (μM)	Excess (μM)	RSD (%)	Added (μM)	Found (μM)	Excess (μM)	RSD (%)
25	15.14	−9.86	4.84	25	60.10	35.10	11.05
50	54.23	4.23	6.64	50	95.94	45.94	11.69
75	72.55	−2.45	7.28	75	118.75	43.75	13.64
100	92.56	−7.44	8.19	100	138.40	38.40	11.42
125	125.19	0.19	6.98	125	166.40	41.40	12.40
150	147.27	−2.73	7.96	150	176.66	26.66	11.66
NaCl				Glyph			
Added (μM)	Found (μM)	Excess (μM)	RSD (%)	Added (μM)	Found (μM)	Excess (μM)	RSD (%)
25	150.71	125.71	9.57	25	183.85	158.85	9.16
50	142.63	92.63	10.36	50	207.39	157.39	8.71
75	197.86	122.86	12.32	75	238.12	163.12	10.60
100	201.21	101.21	11.64	100	252.49	152.49	10.57
125	226.71	101.71	10.83	125	279.68	154.68	8.09
150	287.91	137.91	9.06	150	341.57	191.57	7.86
Co ₃ O ₄							
Control				H ₂ O ₂			
Added (μM)	Found (μM)	Excess (μM)	RSD (%)	Added (μM)	Found (μM)	Excess (μM)	RSD (%)
25	27.48	2.48	6.37	25	53.56	28.56	12.09
50	51.23	1.23	5.78	50	100.93	50.93	12.09
75	72.98	−2.02	6.00	75	111.44	36.44	12.36
100	108.97	8.97	7.45	100	116.64	16.64	11.10
125	129.76	4.75	5.34	125	135.72	10.72	11.51
150	146.65	−3.35	6.03	150	165.81	15.81	11.61
NaCl				Glyph			
Added (μM)	Found (μM)	Excess (μM)	RSD (%)	Added (μM)	Found (μM)	Excess (μM)	RSD (%)
25	155.80	130.80	9.53	25	248.01	223.01	6.94
50	188.75	138.75	12.55	50	272.74	222.74	7.74
75	205.86	130.86	11.12	75	297.92	222.92	7.89
100	233.02	133.02	10.02	100	323.56	223.56	5.81
125	262.04	137.04	10.41	125	348.17	223.17	7.82
150	280.10	130.10	11.25	150	372.80	222.80	4.98

By examining the correlation between the concentration of H₂O₂ released in plants under stress factors (Table 2) and the chlorophyll concentration in samples obtained under the same conditions using optical methods (Table 1), a clear pattern emerged. As the released peroxide increased, there was a noticeable decrease in the chlorophyll concentration. Consequently, the samples subjected to salt and herbicide stress exhibited the lowest chlorophyll concentration and the highest H₂O₂ release concentration. This finding validates that elevated H₂O₂ concentrations in plants lead to a decline in vital functions, and conversely,

an increase in H_2O_2 concentrations can serve as a qualitative and quantitative marker for assessing the impact of external stress on plants.

It can be observed that the relationship of the measured H_2O_2 aligned for both oxides and exhibited an increasing trend from the control sample to the sample exposed to herbicide stress. This consistency enhances the reliability of the findings and further, with appropriate mathematical analysis, facilitates the development of a multisensor system utilizing these two oxides. This system would enable simultaneous measurement and provide precise quantitative values for the concentration of released H_2O_2 .

4. Conclusions

In this article, the process of obtaining nanostructured electrodes CuO and Co_3O_4 on a metal wire was considered. The use of the hydrothermal method made it possible to obtain homogeneous, strong nanostructured coatings that provided a high catalytic reaction, which was used for the non-enzymatic detection of H_2O_2 . The resulting electrodes were highly sensitive, they were characterized by a good linear dependence in a range of concentrations from 20 μM to 7 mM, and they had a high selectivity to the most common interferents found in plant juice. The sensitivity of the obtained CuO electrode was $439.19 \mu\text{A}\cdot\text{mM}^{-1}$. The calculated limit of detection was 1.34 μM . For the Co_3O_4 electrode, the sensitivity was determined to be $505.11 \mu\text{A}\cdot\text{mM}^{-1}$, and the calculated LOD was found to be 1.05 μM .

The morphological parameters of the plants grown under the influence of various stress factors were evaluated. Thus, it turned out that the introduction of small concentrations of H_2O_2 to water for irrigation promoted improved plant growth and an increase in the length of shoots compared to the control ones. In the specimens grown with the addition of NaCl and glyphosate, an inhibition of the shoot length and an increase in the amount of mold in the growth trays were observed, which indicated a general inhibition of vital functions and a decrease in resistance to fungal diseases.

Based on optical measurements, it was observed that the concentration of chlorophyll in the samples exposed to salt and herbicide stress experienced a significant reduction compared to the control sample, with relative changes of 31.5% and 34.5%, respectively. Adding a small amount of H_2O_2 to the irrigation water resulted in a slight increase in the relative concentration of chlorophyll. However, these samples exhibited a higher resilience to the degradation of chlorophyll *a* overtime: the measurements taken on the first day displayed only minor changes compared to the control group, while the measurements conducted after a week revealed a relative change of 28% relative to the control group.

Electrochemical measurements revealed that the control samples exhibited no detectable traces of additional H_2O_2 , indicating the proper functioning of the sensor. In the case of the samples cultivated with low concentrations of H_2O_2 , the average amount of released H_2O_2 was 38.5 μM for CuO and 26.5 μM for Co_3O_4 .

Substantial amounts of H_2O_2 were detected in the samples subjected to NaCl- and glyphosate-induced stress. The CuO electrode demonstrated a more than 110 μM H_2O_2 increase for the NaCl-treated rye samples and a more than 160 μM increase for the glyphosate-treated samples compared to the control sample, while Co_3O_4 exhibited even higher increases of 130 μM and 220 μM , respectively. By examining the relationship between the released H_2O_2 concentration in plants under stress factors and the chlorophyll concentration in the samples obtained under the same conditions using optical methods, a clear pattern emerged. As the released peroxide levels increased, a noticeable decline in the chlorophyll concentration was observed. Consequently, the samples exposed to salt and herbicide stress displayed the lowest chlorophyll concentration and the highest concentration of released H_2O_2 . This finding confirms that elevated H_2O_2 levels in plants contribute to a decrease in vital functions. Conversely, an increase in the H_2O_2 concentration can serve as a qualitative and quantitative indicator for assessing the impact of external stress on plants.

The simultaneous use of CuO and Co₃O₄ nanostructured electrodes coupled with advanced mathematical data processing in future developments will facilitate the creation of a multisensor system. This system will operate with a higher accuracy compared to a single electrode due to its cross-sensitivity capabilities. Furthermore, employing multiple electrodes for hydrogen peroxide detection will enable the simultaneous identification of other substances that can serve as markers for pathological processes.

Author Contributions: Conceptualization, V.G. and I.M.; methodology, M.K., I.M. and V.M.; formal analysis, V.M.; investigation, M.K., I.M., and E.S.; visualization, E.S.; writing—original draft preparation, I.M. and M.K.; writing—review and editing, V.G., E.S. and A.O.; supervision, V.G.; funding acquisition, I.M. All authors have read and agreed to the published version of the manuscript.

Funding: This research was supported by the European Regional Development Fund Activity 1.1.1.2 “Post-doctoral Research Aid”, research agreement no. 1.1.1.2/16/I/001, under grant no. 1.1.1.2/VIAA/4/20/743 “Development of Nanomaterial-based Electrochemical Sensor for Detection of Hydrogen Peroxide”.

Institutional Review Board Statement: Not applicable.

Informed Consent Statement: Not applicable.

Data Availability Statement: The data presented in this study are available on request from the corresponding author.

Conflicts of Interest: The authors declare no conflict of interest.

References

1. Hasanuzzaman, M.; Bhuyan, M.H.M.B.; Zulfiqar, F.; Raza, A.; Mohsin, S.M.; Mahmud, J.A.; Fujita, M.; Fotopoulos, V. Reactive Oxygen Species and Antioxidant Defense in Plants under Abiotic Stress: Revisiting the Crucial Role of a Universal Defense Regulator. *Antioxidants* **2020**, *9*, 681. [CrossRef] [PubMed]
2. Mittler, R.; Zandalinas, S.I.; Fichman, Y.; Van Breusegem, F. Reactive oxygen species signalling in plant stress responses. *Nat. Rev. Mol. Cell Biol.* **2022**, *23*, 663–679. [CrossRef] [PubMed]
3. Tripathy, B.C.; Oelmüller, R. Reactive oxygen species generation and signaling in plants. *Plant Signal Behav.* **2012**, *7*, 1621–1633. [CrossRef]
4. Xie, X.; He, Z.; Chen, N.; Tang, Z.; Wang, Q.; Cai, Y. The Roles of Environmental Factors in Regulation of Oxidative Stress in Plant. *BioMed Res. Int.* **2019**, *2019*, 9732325. [CrossRef]
5. Mansoor, S.; Ali Wani, O.; Lone, J.K.; Manhas, S.; Kour, N.; Alam, P.; Ahmad, A.; Ahmad, P. Reactive Oxygen Species in Plants: From Source to Sink. *Antioxidants* **2022**, *11*, 225. [CrossRef] [PubMed]
6. Smirnov, N.; Arnaud, D. Hydrogen peroxide metabolism and functions in plants. *New Phytol.* **2019**, *221*, 1197–1214. [CrossRef]
7. Choudhury, F.K.; Rivero, R.M.; Blumwald, E.; Mittler, R. Reactive oxygen species, abiotic stress and stress combination. *Plant J.* **2017**, *90*, 856–867. [CrossRef]
8. Hussain, I.; Ashraf, M.A.; Rasheed, R.; Iqbal, M.; Ibrahim, M.; Ashraf, S. Heat shock increases oxidative stress to modulate growth and physico-chemical attributes in diverse maize cultivars. *Int. Agrophys.* **2016**, *30*, 519–531. [CrossRef]
9. Chakraborty, U.; Pradhan, B. Oxidative stress in five wheat varieties (*Triticum aestivum* L.) exposed to water stress and study of their antioxidant enzyme defense system, water stress responsive metabolites and H₂O₂ accumulation. *Braz. J. Plant. Physiol.* **2012**, *24*, 117–130. [CrossRef]
10. Zhang, J.; Lu, M.; Zhou, H.; Du, X.; Du, X. Assessment of Salt Stress to *Arabidopsis* Based on the Detection of Hydrogen Peroxide Released by Leaves Using an Electrochemical Sensor. *Int. J. Mol. Sci.* **2022**, *23*, 12502. [CrossRef]
11. Kar, M. Expression Patterns of Oxidative Stress-Related Genes of Cucurbita pepo and Relation to Cellular H₂O₂ under Short-Term Heavy Metal Stress. *J. Inst. Sci. Tech.* **2020**, *10*, 2952–2961. [CrossRef]
12. González-Sánchez, M.I.; González-Macia, L.; Pérez-Prior, M.T.; Valero, E.; Hancock, J.; Killard, A.J. Electrochemical detection of extracellular hydrogen peroxide in *Arabidopsis thaliana*: A real-time marker of oxidative stress. *Plant Cell Environ.* **2013**, *36*, 869–878. [CrossRef] [PubMed]
13. Baxter, A.; Mittler, R.; Suzuki, N. ROS as key players in plant stress signaling. *J. Exp. Bot.* **2014**, *65*, 1229–1240. [CrossRef]
14. Kuźniak, E.; Urbanek, H. The involvement of hydrogen peroxide in plant responses to stresses. *Acta Physiol. Plant.* **2000**, *22*, 195–203. [CrossRef]
15. Lin, C.C.; Kao, C.H. Effect of NaCl stress on H₂O₂ metabolism in rice leaves. *Plant Growth Regul.* **2000**, *30*, 151–155. [CrossRef]
16. Cheeseman, J.M. Hydrogen Peroxide and Plant Stress: A Challenging Relationship. *Plant Stress (Glob. Sci. Books)* **2007**, *1*, 4–15. Available online: [http://www.globalsciencebooks.info/Online/GSBOonline/images/0706/PS_1\(1\)/PS_1\(1\)4-15o.pdf](http://www.globalsciencebooks.info/Online/GSBOonline/images/0706/PS_1(1)/PS_1(1)4-15o.pdf) (accessed on 5 July 2023).
17. Carril, P.; da Silva, A.B.; Tenreiro, R.; Cruz, C. An Optimized in situ Quantification Method of Leaf H₂O₂ Unveils Interaction Dynamics of Pathogenic and Beneficial Bacteria in Wheat. *Front. Plant Sci.* **2020**, *11*, 889. [CrossRef]

18. Liu, S.; Yang, R. Chapter 14—Regulations of reactive oxygen species in plants abiotic stress: An integrated overview. In *Plant Life under Changing Environment: Responses and Management*; Tripathi, D.K., Singh, V.P., Chauhan, D.K., Sharma, S., Prasad, S.M., Dubey, N.K., Ramawat, N., Eds.; Academic Press: Cambridge, MA, USA, 2020; pp. 323–353. [[CrossRef](#)]
19. Sharma, P.; Jha, A.B.; Dubey, R.S.; Pessarakli, M. Reactive Oxygen Species, Oxidative Damage, and Antioxidative Defense Mechanism in Plants under Stressful Conditions. *J. Bot.* **2012**, *2012*, 217037. [[CrossRef](#)]
20. Guler, N.S.; Pehlivan, N. Exogenous low-dose hydrogen peroxide enhances drought tolerance of soybean (*Glycine max* L.) through inducing antioxidant system. *Acta Biol. Hung.* **2016**, *67*, 169–183. [[CrossRef](#)]
21. Qamer, Z.; Chaudhary, M.T.; Du, X.; Hinze, L.; Azhar, M.T. Review of oxidative stress and antioxidative defense mechanisms in *Gossypium hirsutum* L. in response to extreme abiotic conditions. *J. Cotton Res.* **2021**, *4*, 9. [[CrossRef](#)]
22. Zhu, H.; Jia, Z.; Trush, M.A.; Li, Y.R. A Highly Sensitive Chemiluminometric Assay for Real-Time Detection of Biological Hydrogen Peroxide Formation. *React. Oxyg. Species (Apex NC)* **2016**, *1*, 216–227. [[CrossRef](#)]
23. Ostaszewski, R.; Wilk, M. Efficient assay for the detection of hydrogen peroxide via estimation of the enzyme promiscuous activity in the perhydrolysis reaction. *ChemBioChem* **2020**, *22*, 1464–1469. [[CrossRef](#)]
24. Cohn, C.A.; Pak, A.; Strongin, D.; Schoonen, M.A. Quantifying hydrogen peroxide in iron-containing solutions using leuco crystal violet. *Geochem. Trans.* **2005**, *6*, 47–51. [[CrossRef](#)]
25. Eisenberg, G.M. Colorimetric Determination of Hydrogen Peroxide. *Ind. Eng. Chem. Anal. Ed.* **1943**, *15*, 327–328. [[CrossRef](#)]
26. Leichnetz, S.; Heinrich, J.; Kulak, N. A Fluorescence Assay for the Detection of Hydrogen Peroxide and Hydroxyl Radicals generated by Metallonucleases. *Chem. Commun.* **2018**, *54*, 13411–13414. [[CrossRef](#)]
27. Kim, H.; Xue, X. Detection of Total Reactive Oxygen Species in Adherent Cells by 2',7'-Dichlorodihydrofluorescein Diacetate Staining. *J. Vis. Exp.* **2020**, *160*, e60682. [[CrossRef](#)]
28. Cai, H.; Liu, X.; Zou, J.; Xiao, J.; Yuan, B.; Li, F.; Cheng, Q. Multi-wavelength spectrophotometric determination of hydrogen peroxide in water with peroxidase-catalyzed oxidation of ABTS. *Chemosphere* **2018**, *193*, 833–839. [[CrossRef](#)]
29. Wang, M.; Qiu, S.; Yang, H.; Huang, Y.; Dai, L.; Zhang, B.; Zou, J. Spectrophotometric determination of hydrogen peroxide in water with peroxidase-catalyzed oxidation of potassium iodide and its applications to hydroxylamine-involved Fenton and Fenton-like systems. *Chemosphere* **2021**, *270*, 129448. [[CrossRef](#)]
30. Huo, D.; Li, D.; Xu, S.; Tang, Y.; Xie, X.; Li, D.; Song, F.; Zhang, Y.; Li, A.; Sun, L. Disposable Stainless-Steel Wire-Based Electrochemical Microsensor for In Vivo Continuous Monitoring of Hydrogen Peroxide in Vein of Tomato Leaf. *Biosensors* **2022**, *12*, 35. [[CrossRef](#)]
31. Fernando, C.D.; Soysa, P. Optimized enzymatic colorimetric assay for determination of hydrogen peroxide (H₂O₂) scavenging activity of plant extracts. *MethodsX* **2015**, *2*, 283–291. [[CrossRef](#)]
32. Patel, V.; Kruse, P.; Selvaganapathy, P.R. Solid State Sensors for Hydrogen Peroxide Detection. *Biosensors* **2021**, *11*, 9. [[CrossRef](#)]
33. Zhao, F.; Zhou, S.; Zhang, Y. Ultrasensitive Detection of Hydrogen Peroxide Using Bi₂Te₃ Electrochemical Sensors. *ACS Appl. Mater. Interfaces.* **2021**, *13*, 4761–4767. [[CrossRef](#)] [[PubMed](#)]
34. Murugan, P.; Sundramoorthy, A.K.; Nagarajan, R.D.; Atchudan, R.; Shanmugam, R.; Ganapathy, D.; Arya, S.; Alothman, A.A.; Ouladsmame, M. Electrochemical detection of H₂O₂ on graphene nanoribbons/cobalt oxide nanorods-modified electrode. *J. Nanomater.* **2022**, *2022*, 9866111. [[CrossRef](#)]
35. Mariani, F.; Gualandi, I.; Schuhmann, W.; Scavetta, E. Micro- and nano-devices for electrochemical sensing. *Microchim. Acta* **2022**, *189*, 459. [[CrossRef](#)]
36. Rismetov, B.; Ivandini, T.A.; Saepudin, E.; Einaga, Y. Electrochemical detection of hydrogen peroxide at platinum-modified diamond electrodes for an application in melamine strip tests. *Diam. Relat. Mater.* **2014**, *48*, 88–95. [[CrossRef](#)]
37. Ahmad, T.; Iqbal, A.; Halim, S.A.; Uddin, J.; Khan, A.; El Deeb, S.; Al-Harrasi, A. Recent Advances in Electrochemical Sensing of Hydrogen Peroxide (H₂O₂) Released from Cancer Cells. *Nanomaterials* **2022**, *12*, 1475. [[CrossRef](#)]
38. Shin, J.H.; Lee, M.J.; Choi, J.H.; Song, J.A.; Kim, T.H.; Oh, B.K. Electrochemical H₂O₂ biosensor based on horseradish peroxidase encapsulated protein nanoparticles with reduced graphene oxide-modified gold electrode. *Nano Converg.* **2020**, *7*, 39. [[CrossRef](#)]
39. Atacan, K.; Özacar, M. Construction of a non-enzymatic electrochemical sensor based on CuO/g-C₃N₄ composite for selective detection of hydrogen peroxide. *Mater. Chem. Phys.* **2021**, *266*, 124527. [[CrossRef](#)]
40. Rajendran, S.; Manoj, D.; Suresh, R.; Vasseghian, Y.; Ghfar, A.A.; Sharma, G.; Soto-Moscoso, M. Electrochemical detection of hydrogen peroxide using micro and nanoporous CeO₂ catalysts. *Environ. Res.* **2022**, *214 Pt 3*, 113961. [[CrossRef](#)]
41. Shamkhalichenar, H.; Choi, J.W. Review—Non-Enzymatic Hydrogen Peroxide Electrochemical Sensors Based on Reduced Graphene Oxide. *J. Electrochem. Soc.* **2020**, *167*, 037531. [[CrossRef](#)]
42. Terán-Alcocer, Á.; Bravo-Plascencia, F.; Cevallos-Morillo, C.; Palma-Cando, A. Electrochemical Sensors Based on Conducting Polymers for the Aqueous Detection of Biologically Relevant Molecules. *Nanomaterials* **2021**, *11*, 252. [[CrossRef](#)] [[PubMed](#)]
43. Curulli, A. Nanomaterials in Electrochemical Sensing Area: Applications and Challenges in Food Analysis. *Molecules* **2020**, *25*, 5759. [[CrossRef](#)]
44. Krasovska, M.; Gerbreders, V.; Mihailova, I.; Ogurcovs, A.; Sledevskis, E.; Gerbreders, A.; Sarajevs, P. ZnO-nanostructure-based electrochemical sensor: Effect of nanostructure morphology on the sensing of heavy metal ions. *Beilstein J. Nanotechnol.* **2018**, *9*, 2421–2431. [[CrossRef](#)]

45. Wang, K.; Sun, Y.; Xu, W.; Zhang, W.; Zhang, F.; Qi, Y.; Zhang, Y.; Zhou, Q.; Dong, B.; Li, C.; et al. Non-enzymatic electrochemical detection of H₂O₂ by assembly of CuO nanoparticles and black phosphorus nanosheets for early diagnosis of periodontitis. *Sens. Actuators B Chem.* **2022**, *355*, 131298. [[CrossRef](#)]
46. Trujillo, R.M.; Barraza, D.E.; Zamora, M.L.; Cattani-Scholz, A.; Madrid, R.E. Nanostructures in Hydrogen Peroxide Sensing. *Sensors* **2021**, *21*, 2204. [[CrossRef](#)] [[PubMed](#)]
47. Thatikayala, D.; Ponnamma, D.; Sadasivuni, K.K.; Cabibihan, J.-J.; Al-Ali, A.K.; Malik, R.A.; Min, B. Progress of Advanced Nanomaterials in the Non-Enzymatic Electrochemical Sensing of Glucose and H₂O₂. *Biosensors* **2020**, *10*, 151. [[CrossRef](#)] [[PubMed](#)]
48. Peña, R.C.; Silva, V.O.; Quina, F.H.; Bertotti, M. Hydrogen peroxide monitoring in Fenton reaction by using a ruthenium oxide hexacyanoferrate/multiwalled carbon nanotubes modified electrode. *J. Electroanal. Chem.* **2012**, *686*, 1–6. [[CrossRef](#)]
49. Urban, S.; Weltin, A.; Flamm, H.; Kieninger, J.; Deschner, B.J.; Kraut, M.; Dittmeyer, R.; Urban, G.A. Electrochemical multisensor system for monitoring hydrogen peroxide, hydrogen and oxygen in direct synthesis microreactors. *Sens. Actuators B Chem.* **2018**, *273*, 973–982. [[CrossRef](#)]
50. Pauliukaite, R.; Voitechovič, E. Multisensor Systems and Arrays for Medical Applications Employing Naturally-Occurring Compounds and Materials. *Sensors* **2020**, *20*, 3551. [[CrossRef](#)]
51. Mihailova, I.; Gerbreders, V.; Krasovska, M.; Sledevskis, E.; Mizers, V.; Bulanovs, A.; Ogurcovs, A. A non-enzymatic electrochemical hydrogen peroxide sensor based on copper oxide nanostructures. *Beilstein J. Nanotechnol.* **2022**, *13*, 424–436. [[CrossRef](#)]
52. Arnon, D.I. Copper enzymes in isolated chloroplasts. Polyphenoloxidase in *Beta vulgaris*. *Plant Physiol.* **1949**, *24*, 1–15. [[CrossRef](#)] [[PubMed](#)]
53. Shinde, S.; Paralikar, P.; Ingle, A.P.; Rai, M. Promotion of seed germination and seedling growth of Zea mays by magnesium hydroxide nanoparticles synthesized by the filtrate from *Aspergillus niger*. *Arab. J. Chem.* **2020**, *13*, 3172–3182. [[CrossRef](#)]
54. Kokina, I.; Plaksenkova, I.; Galek, R.; Jermałonoka, M.; Kirilova, E.; Gerbreders, V.; Krasovska, M.; Sledevskis, E. Genotoxic Evaluation of Fe₃O₄ Nanoparticles in Different Three Barley (*Hordeum vulgare* L.) Genotypes to Explore the Stress-Resistant Molecules. *Molecules* **2021**, *26*, 6710. [[CrossRef](#)] [[PubMed](#)]

Disclaimer/Publisher's Note: The statements, opinions and data contained in all publications are solely those of the individual author(s) and contributor(s) and not of MDPI and/or the editor(s). MDPI and/or the editor(s) disclaim responsibility for any injury to people or property resulting from any ideas, methods, instructions or products referred to in the content.